

# First speckle-interferometry at SOAR telescope with electron multiplication CCD

A. Tokovinin and R. Cantarutti

*Cerro Tololo Inter-American Observatory, Casilla 603, La Serena, Chile*

atokovinin@ctio.noao.edu, rcantarutti@ctio.noao.edu

## ABSTRACT

A simple camera with electron-multiplication CCD, fast frame rate, and pixel scale of 15 mas is described. This instrument was tested at the SOAR 4-m telescope in speckle interferometry regime. The data were processed by the standard speckle algorithm permitting to derive binary-star parameters. We observed 29 objects with separations from 21 mas to  $1''32$ , mostly southern binaries with known orbits. Some pairs require orbit revision. Two spectroscopic binaries HIP 9631 and HIP 11072 and the astrometric binary  $\kappa$  For are resolved for the first time, three objects were unresolved.

*Subject headings:* Astronomical Instrumentation

## 1. Introduction

High angular resolution opens new horizons for astronomy, as amply demonstrated by the success of the Hubble Space Telescope (HST) in the UV and visible and by adaptive optics (AO) in the near-infrared. However, not all problems can be tackled by the aging HST. One way to enhance the resolution and sensitivity of ground-based optical astronomy is by partial compensation of low-altitude turbulence (ground-layer AO). SOAR Adaptive Module (SAM) instrument (Tokovinin et al. 2004) is being built for the 4-m SOAR telescope to materialize this gain. Full AO compensation in the visible is still beyond the reach, as it would require either a bright natural guide star or a powerful and expensive laser system.

Speckle interferometry permits to attain diffraction-limited resolution in the visible even without full AO correction, e.g. Horch et al. (1997). The sensitivity of this method critically depends on the seeing. We realize that even a partial correction delivered by SAM increases the number of photons per speckle by a factor of two or more, thus boosting the sensitivity of speckle-interferometry beyond its standard limits. To exploit this opportunity and to help in the technical work with the

SAM instrument, we built a small *High-Resolution Camera* (HRCam) instrument with an electron-multiplication CCD (EM CCD) as a detector.

This paper reports on the first of HRCam tests, still without AO correction. We observed a set of binary stars, mostly with well-known orbits, for evaluating the potential of speckle-interferometry with HRCam. Apart from this purely technical goal, we did resolve some stars for the first time, so the results of these tests seem worth of publishing. § 2 describes the HRCam, § 3 – observations and data reduction. The results are presented in § 4 and discussed in § 5.

## 2. Instrument description

The HRCam detector is a EM CCD *Luca* from Andor<sup>1</sup>, selected for its low cost, fast frame rate, and simple signal interface via a USB port. This detector has already been used at SOAR by Cecil & Rashkeev (2007) for imaging Mercury. Even though the stars observed in speckle interferometry are relatively bright, the number of photons per pixel received in a single short exposure is often less than one. Electron multiplication effec-

---

<sup>1</sup>www.andor.com

tively reduces the readout noise to levels below 1 electron, so the sensitivity of speckle interferometry becomes photon-limited. In the case of bare CCDs, it is limited by the readout noise.

The pixel size of Luca is  $10\ \mu\text{m}$ . The size of the diffraction-limited speckle  $\lambda/D$  is 25 mas at 500 nm and 33 mas at 656 nm ( $D = 4.1\ \text{m}$  is the telescope diameter,  $\lambda$  is the wavelength), so, to Nyquist-sample these images, we need an angular pixel scale of about 15 mas. In the HRCam, the  $F/16$  beam of SOAR is collimated by a 50-mm negative achromat (Barlow lens) and refocused by a 100-mm positive lens, doubling the effective telescope focal length. Additional benefit of this solution is a collimated space between the lenses where filters can be placed without introducing focus changes. So far, we installed the standard *BVRI* filter set complemented by an  $\text{H}\alpha$  filter ( $\lambda_{\text{max}} = 657\ \text{nm}$ ,  $\Delta\lambda_{\text{FWHM}} = 5.05\ \text{nm}$ , transmission 0.80). The detector is not sensitive in the  $U$  band. Major parameters of HRCam are listed in Table 1.

Atmospheric dispersion is corrected in most speckle cameras by Risley prisms. The SAM instrument will be equipped with a dispersion corrector, so HRCam has none. In the test run reported here, we used only the  $\text{H}\alpha$  filter to get rid of the dispersion, while penalizing the sensitivity by a narrow bandwidth. With this filter, atmospheric dispersion elongates speckles by only 12 mas FWHM (5 mas rms) at zenith distance  $45^\circ$  and therefore can be neglected.

The Luca detector can work as a normal CCD, without EM gain. In this regime, we measured the response of 1.7 electrons per analogue-to-digital unit (ADU) and a readout noise of 8.4 ADU. The

non-linear correspondence between the EM gain setting in the camera and the actual EM gain was established experimentally. For the gain setting of 200 used here, the actual EM gain is about 40, so the effective readout noise is only 0.35 el. The EM amplification introduces additional noise which increases the signal variance by 1.7 times, compared to pure photon noise. The signal in the  $V$  band corresponds to the detector quantum efficiency (QE) around 0.5.

The Luca manufacturer provides a software development kit (SDK) for controlling the camera under Linux operating system. We used this SDK and created a software with a graphic user interface that has all functionality required for HRCam operation. The data are saved as 3-dimensional FITS cubes in 2-byte unsigned-integer format. All parameters of the detector and filters are saved in the headers, as well as the relevant information from the telescope. Note that Cecil & Rashkeev (2007) used for Mercury observations the manufacturer’s software under Windows.

We checked that in the fast continuous acquisition mode (kinetic mode), the temporal sampling is regular, without random gaps caused by the software. For example, we acquired 1-ms exposures of a  $100\times 100$  pixel region-of-interest (ROI) with a frame rate of 50 Hz and found that the actual sampling time was 22 ms instead of 20 ms. The temporal regularity is not important for speckle interferometry but matters for other applications such as vibration analysis or fast photometry.

We found that the signal level corresponding to the zero flux (bias) is stable and uniform when acquiring single images. However, in the kinetic mode the bias level shows a strong variation in the vertical direction (along CCD columns). This is a feature of the Luca camera itself, not of the acquisition software, as it was evidenced both under Windows and under Linux. The bias pattern depends on the exposure time, sampling time, and ROI parameters. We found that it is more uniform when the interval between successive frames is minimized, i.e. when the detector runs at its maximum speed. To simplify data processing, we recorded empty frames with the same settings as the data frames and subtracted average bias from the data. This procedure automatically removes any dark current. With the detector cooled to its

Table 1: Summary of HRCam parameters

Parameter	Value
Pixel scale	15 mas
Format	658x496, $9.9'' \times 7.5''$
Signal resolution	14 bits, 1.7 el/ADU
Readout noise	14.3 el or 8.4 ADU
QE	0.5 (max)
EM gain	1 to 440
Readout speed	$30\ \text{s}^{-1}$ full-frame
Filters	B, V, R, I, $\text{H}\alpha$

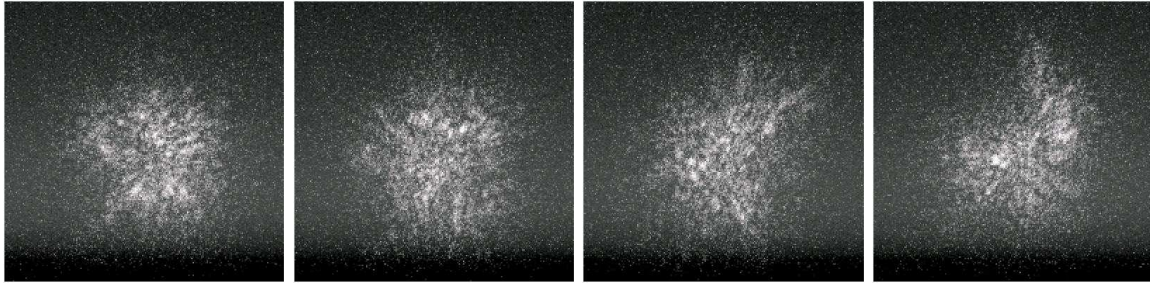


Fig. 1.— Five consecutive speckle frames of HR 350 ( $V = 6.41$ ). Logarithmic intensity scaling, field of view  $3'' \times 3''$ .

nominal temperature of  $-20^\circ\text{C}$ , the dark current is conspicuous only in a small number ( $\sim 500$ ) of “hot” pixels, reaching values of 50–100 el/s, and very low in the remaining 99.8% of pixels. Averaged over all pixels, the dark current is about 0.1 el/s.

A flat field image obtained in the laboratory shows the rms scatter of 0.6% in a central  $200 \times 200$  ROI, with peak deviations of  $-3.0\%$  and  $+1.6\%$ . With such a good detector cosmetic quality, no flat-field correction seems necessary for the speckle work. We tested the HRCam and its software by acquiring series of speckle images simulated in the laboratory with a laser beam and a moving random phase screen. Processing of these data shows a very good match between the measured power spectrum and its theoretical model.

### 3. Observations and data processing

The data reported here were obtained on October 24/25 2007 (2007.813), on the first night of HRCam tests. The camera was installed at the “IR-straight” Nasmyth port of the SOAR telescope. The instrument rotator provided constant orientation of the detector on the sky, compensating the field rotation produced by the SOAR alt-azimuth mount. All speckle data are obtained through the  $H\alpha$  filter using a EM gain of 40.

The sky was clear, the seeing reported by the site monitor was good ( $0''.5 - 0''.7$ ), and the wind was weak. These benign conditions helped to adjust the focus accurately and to keep the images well centered. We selected a  $200 \times 200$  square ROI ( $3''$  on the sky) and acquired images with 20 ms exposure time with a nominal time sampling of 50 ms. Each data cube contains from 200 to 400

images.

Figure 1 shows a representative sample of single-star speckle frames. The bias is not subtracted and is seen as a dark feature in the lower part of the frames. The 50-ms sampling time was sufficiently long, so the speckle images are uncorrelated.

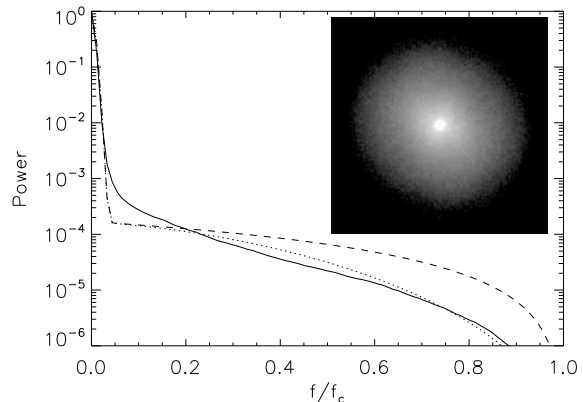


Fig. 2.— Power spectrum of the single star HR 1338 is radially averaged and plotted in full line in comparison with the model (1) with  $D/r_0 = 50.8$  (dashed line). The dotted line is the same model with additional Gaussian blur of 13 mas rms. The insert shows the 2-dimensional spectrum with logarithmic intensity scale in the range  $10^{-6}$  to  $10^{-3}$ .

The data are processed by the standard speckle method, e.g. (Horch et al. 1997), with an IDL code written for the purpose. At the first pass, the average bias is subtracted and the power spectrum is accumulated and saved. The power spectra  $P(\mathbf{f})$ , normalized so that  $P(0) = 1$ , are dominated by a strong peak at low frequencies

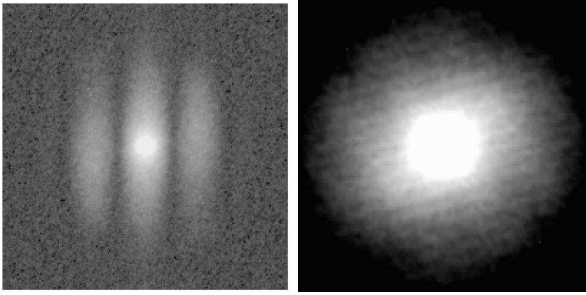


Fig. 3.— Power spectra of binary stars. Left: binary HIP 22573 = Fin 320, separation 77 mas,  $\Delta m = 0.49$ . Right: newly resolved binary HIP 11072 =  $\kappa$  For (0.52'',  $\Delta m = 6.0$ ).

(LF, “seeing” component) and an extended high-frequency (HF) halo corresponding to the speckle structure. Figure 2 shows a typical power spectrum of a single star  $P_0(\mathbf{f})$  (reference source), with noise bias subtracted. A simple theory (Dainty & Greenaway 1979) predicts that  $P_0(\vec{f})$  can be modeled as

$$P_0(f) \approx \exp[-3.44(f/f_c)^{5/3} (D/r_0)^{5/3}] + 0.435(D/r_0)^{-2}T_0(f), \quad (1)$$

where  $f = |\mathbf{f}|$  is the modulus of the spatial frequency,  $D = 4.1$  m is the telescope diameter,  $f_c = D/\lambda$  is the cutoff frequency,  $r_0$  is the Fried parameter, and  $T_0(f)$  is the diffraction-limited transfer function,  $T_0(f) = 2/\pi[\arccos(f/f_c) - (f/f_c)\sqrt{1 - (f/f_c)^2}]$  for  $f < f_c$  and zero otherwise. We adjust the single parameter of this model,  $D/r_0$ , either to the width of the LF part or to the level of  $P_0(0.2f_c)$  and obtain similar values by these two methods. For our data set,  $D/r_0$  varied between 36 and 50, which corresponds to the seeing  $\epsilon = 0.98\lambda/r_0$  in the range 1''.16 to 1''.62 (at 656 nm). The FWHM size of average stellar images was smaller, from 0''.7 to 1''.

Figure 2 demonstrates that the single-star power spectrum declines faster than predicted by the model (1). Despite different values of  $D/r_0$ , the HF part of the spectra is almost the same for all reference stars and reaches  $10^{-6}$  level at about  $0.9f_c$ . We suspect that additional damping of the HF power is caused mostly by small telescope vibrations, as found previously at other telescopes used for speckle interferometry (Altarc et al. 2001). The dotted line in Fig. 2 includes

in the model an additional Gaussian filter corresponding to the 13 mas rms blur. Data from the SOAR fast tip-tilt guider provided by M. Warner indicate that vibration of comparable amplitude is indeed expected in 20-ms exposures. On the other hand, the degree and orientation of the asymmetry do not correlate with the zenith distance and parallactic angle, so it is not caused by the atmospheric dispersion, which is too small anyway to explain the effect. In the cases when the HF part is non-isotropic, the disagreement with the model is larger. Vibrations decrease the sensitivity of speckle-interferometry with respect to the theoretical predictions and contribute to the differences between object and reference.

When the star is a binary, the power spectrum is modulated by fringes. Two such examples are shown in Fig. 3 with intensity scaling that brings out the HF component. In few cases when the bias subtraction left a residual variation in the vertical direction, the power spectra have a bright vertical stripe at the center. The absence of such feature in Fig. 3 shows that the bias subtraction worked well.

At the second pass through the data, the binary parameters are extracted from the power spectra. The actual sampling was  $k = 2.2$  pixels per  $\lambda/D$ . The bias level in the power spectrum produced by the photon and readout noise,  $P_{\text{noise}}$ , was calculated by averaging at spatial frequencies beyond the cutoff frequency  $f_c = D/\lambda$ , i.e. at a radius beyond  $N/k = 91$  pixels from the coordinate center, where  $N = 200$  is the image size. We subtract the noise bias from the power spectrum, removing its potential effect on the calculation of magnitude difference. The same procedure is applied to the power spectra of single (reference) stars. Apart from the noise bias, we eliminated 6 bright pixels at fixed positions apparently caused by a fixed-pattern noise in the detector.

The binary parameters of interest are the separation  $\rho$ , position angle  $\theta$  and magnitude difference  $\Delta m$ . The first two numbers are combined in a 2-dimensional vector  $\mathbf{r}$ . The observed power spectrum  $P(\mathbf{f})$  is fitted by a model

$$P(\mathbf{f}) = P_0(\mathbf{f}) [A + B \cos(2\pi\mathbf{f}\mathbf{r})], \quad (2)$$

where  $P_0(\mathbf{f})$  is the power spectrum of the single reference star, while the coefficients  $A$  and  $B$  define the relative scaling and the magnitude differ-

ence. If the intensity ratio of the binary components is  $\alpha = 10^{-0.4\Delta m}$ , then  $\beta = B/A = 2\alpha/(1 + \alpha^2)$ . Inverting this equation, we calculate the intensity ratio (hence  $\Delta m$ ) as  $\alpha = (1 - \sqrt{1 - \beta^2})/\beta$ . Note that the sensitivity of the measured quantity  $\beta$  to  $\Delta m$  diminishes for binaries with  $\Delta m \sim 0$ , so the relative photometry of nearly equal components must be imprecise and possibly biased.

The fitting is done by the non-linear Levenberg-Marquardt method (Press et al. 1992). Only the HF portion of the power spectra from  $0.1f_c$  to  $0.8f_c$  is used in the fit, and only the upper half of the frequency plane matters due to the symmetry. In order to get converging fits, a good initial estimate of the binary parameters and a good model of measurement errors are essential. It is known that the signal-to-noise ratio in a single-image power spectrum is one. Hence, we adopt the errors  $\sigma_P = (|P| + P_{\text{noise}})M^{-1/2}$ , i.e. take into consideration the noise bias and the number of frames in the data cube  $M$ . The quality of the fit is then evaluated by the parameter  $\chi^2/\nu$ , where  $\chi^2$  is the sum of squared residuals normalized by  $\sigma_P^2$  and  $\nu$  is the number of the fitted points in the power spectrum. We neglect the errors in the reference spectrum  $P_0(\mathbf{f})$ . If these errors were similar to the errors in the binary power spectrum, the fit quality parameter  $\chi^2/\nu$  would be simply doubled. However, the reference is usually bright (smaller errors), while the difference between object and reference is almost always dominated by systematic effects rather than by random errors. In our fits,  $\chi^2/\nu$  ranges from 0.7 to 10, with few exceptions.

The initial estimate of the parameters ( $\mathbf{r}$ ,  $A$ ,  $B$ ) is done automatically. The binary components produce peaks in the auto-correlation function (ACF), which is the Fourier transform of the power spectrum. However, narrow speckle peaks in the ACF of speckle images are superimposed on a wide “seeing” pedestal, complicating automatic identification of the components. To alleviate the problem, we set to zero the power spectrum inside the circle  $|\mathbf{f}| < 0.1f_c$ , i.e. use high-pass filtering to “kill” the seeing pedestal. Such brutal filtering results in ringing (Fig. 4), but brings up the companions clearly. The companion is identified as a global maximum of the filtered ACF outside some pre-defined radius (usually 2 pixels), to avoid the central peak. The ratio of the binary peak to the

central peak is equal to  $B/(2A)$  and serves for the initial estimate of the parameter  $B$  in eq. 2. The parameter  $A$  is simply a ratio between the average values of the object and reference power spectra. Thus, the initial parameters for the fit are fully defined. In complicated cases (e.g. very close binaries) we set the initial  $\mathbf{r}$  estimate manually.

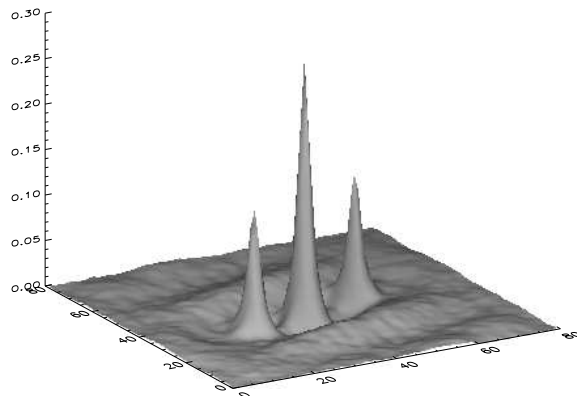


Fig. 4.— Example of high-pass filtered ACF: HIP 2941 ( $0''.24$ ,  $\Delta m = 0.56$ ). Only the central part of the ACF is displayed.

Each object has from 2 to 5 independent data cubes which were processed individually. The final estimates of  $(\rho, \theta, \Delta m)$  are obtained simply by averaging the results, while the measurement errors of these parameters (including  $\Delta m$ ) are estimated by the scatter about the average. The smallness of these errors (typically  $\sigma_\rho < 1$  mas) indicates good internal agreement of our results. The external errors are likely dominated by the systematic effects not accounted for, such as mismatch between reference and object.

#### 4. Results

Table 2 lists the measured binary parameters. Each object is identified by its WDS J2000 code (Mason et al. 2001) and number in the HIPPARCOS catalog (ESA 1997). The separations are converted from pixels to arcseconds using the pixel scale 14.8 mas, the angles were corrected by adding the instrumental offset  $3.5^\circ$  to the measurements (see below). Three unresolved stars are listed with UR in place of the separation.

No special measures to calibrate the detector

Table 2: Binary star measurements (epoch 2007.813, wavelength 657 nm)

WDS J2000	HIP	Name	$\rho$ , mas	$\theta$ , °	$\Delta m$	$N_{\text{obs}}$	$\rho_{\text{eph}}$ mas	$\theta_{\text{eph}}$ °	Gr	$\Delta \text{Hp}$
00352-0336	2762	HO 212AB	39.1±1.0	33.1±1.4	1.09±0.08	5	41.8	28.6	-1	
00373-2446	2941	BU 395	238.0 0.4	74.7 0.0	0.56 0.01	3	240.5	68.9	-1	0.32
01084-5515	5348	RST1205AB	533.3 0.8	107.5 0.1	2.89 0.02	3	520.4	108.9	5	2.78
01361-2954	7463	HJ 3447	763.4 0.4	179.5 0.1	1.30 0.04	4	805.4	182.3	-5	1.29
01376-0924	7580	KUI 7	117.4 0.1	129.5 0.1	1.11 0.02	3	115.4	128.7	2	
02038-0021	9631	new	46.0 2.8	98.7 2.6	1.82 0.07	4				
02128-0224	10305	new	21.2 1.5	115.4 2.4	0.51 0.12	5				
02225-2349	11072	kap For	542.4 6.5	105.9 1.2	6.00 0.28	3	428.6	119.1	-9	
02396-1152	12390	FIN 312	113.1 0.1	263.8 0.1	0.68 0.02	4	117.7	260.1	1	
02460-0457	12812	BU 83	916.3 0.4	15.5 0.1	1.83 0.02	3	815.3	14.8	5	1.86
03003-1118	-	A 2611	183.7 1.0	38.7 0.2	1.53 0.03	3	88.8	80.8	-4	
03124-4425	14913	JC 8AB	678.4 0.4	162.7 0.0	0.76 0.01	3	702.8	163.2	3	0.71
03184-2231	15382	SEE 23	330.6 0.2	97.9 0.1	1.84 0.01	3	295.0	100.4	3	1.25
03244-1539	15868	A 2909AB	UR			2	146.9	25.6	-4	
03339-3105	16628	B 52	278.6 0.2	322.3 0.1	0.94 0.01	3	278.5	323.6	3	0.93
03339-5234	19248	-	UR			2				
03544-4022	18262	FIN 344	24.5 1.0	81.0 1.7	1.10 0.08	4				
04142-4608	19758	RST2338	233.5 0.6	286.0 0.1	1.27 0.02	3	239.3	286.7	3	1.29
04395-4507	21698	I 1489	204.9 0.9	90.9 0.2	1.09 0.01	2	163.2	100.7	-4	0.79
04515-3454	22573	FIN 320	76.7 0.4	182.6 0.0	0.49 0.01	2	126.6	122.7	-3	
05045-3542	23596	HDS 658	906.7 0.6	11.9 0.1	3.01 0.07	3				3.11
05190-2159	24800	RST2375	176.8 0.1	8.6 0.1	0.90 0.02	2	196.7	358.9	-4	0.81
05239-0052	25240	A 847BC	84.3 0.1	213.2 0.2	0.43 0.08	2	14.6	216.0	-2	
05245-0224	25281	MCA 18Aa	40.1 0.6	284.1 0.9	1.48 0.04	2	51.7	297.3	-3	
05319-7620	25918	-	UR			2	65.0	97.5	-9	
05532-6150	27822	SLR 15	441.3 0.0	117.6 0.0	0.74 0.00	2	305.6	103.7	-5	0.67
06003-3102	28442	HU 1399AB	734.1 0.8	119.6 0.0	1.14 0.13	2	741.0	120.4	4	0.96
06003-3102	28442	HJ 2823CE	354: 1.8	139.1 0.3	3.90: 0.18	2	410.0	81.2	-5	
22266-1645	110778	SHJ 345AB	1325.0 1.0	30.9 0.0	0.72 0.05	3	1368.8	30.2	4	0.15

pixel scale and orientation were taken during this first test run. We calibrate the results *a posteriori* by comparing with ephemeris positions for binaries with known orbits. The orbital elements were extracted from the on-line version of the Sixth Catalog (VB6) by Hartkopf et al. (2001) and the positions for 2007.813 were computed for each binary without accounting for the precession. The measured position angles  $\theta$  were changed by  $180^\circ$  whenever indicated by the ephemeris, otherwise they are in the range  $0^\circ - 180^\circ$  because standard speckle processing does not distinguish between symmetrical configurations. The calculated ephemeris positions are given in the last columns of Table 2.

The quality of the orbits in VB6 is graded on a scale from 1 (best) to 5 (preliminary). However, there is no unique relation between grades and ac-

curacy of the ephemeris positions. A wide binary with an orbit of grade 5 can have a very accurate ephemeris, while a close binary with orbit of grade 1 can show large residuals. We eliminated from the calibration all close binaries with  $\rho < 0''.1$  and binaries with large residuals and marked such discarded systems by negative grades in Table 2. For the remaining 10 systems, the corrections in pixel scale and position angle were determined as weighted average, with weights inversely proportional to the squared errors. Assigning errors to the ephemeris position is a guesswork, of course. We adopted arbitrarily the ephemeris errors  $\sigma_\theta = 0.5^\circ \rho^{-1} G^{1/2}$  and  $\sigma_\rho = (0.01'' + 0.005\rho) G^{1/2}$ , where  $G$  is the orbit grade and  $\rho$  is the separation in arcseconds.

As a result of the calibration, we determined the position angle offset of  $3.5^\circ \pm 1.7^\circ$  and a correc-

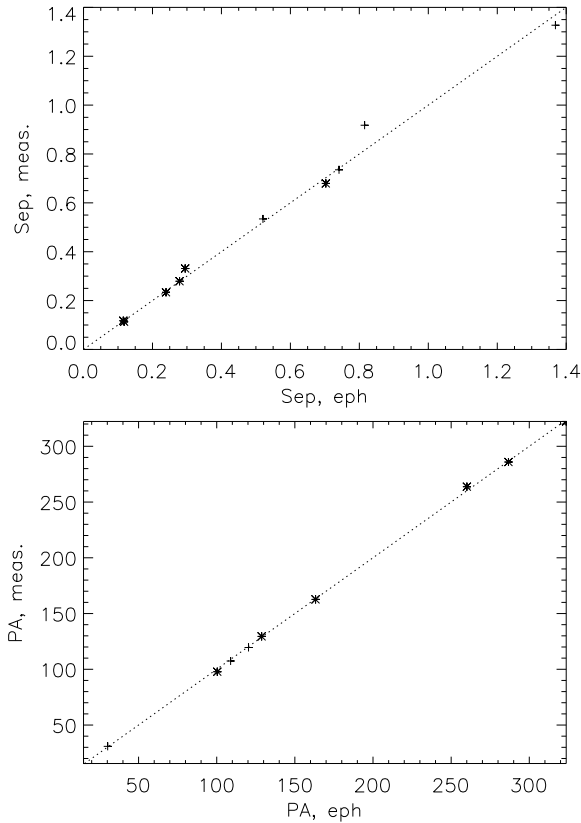


Fig. 5.— Comparison between measured positions (vertical axis) and ephemeris (horizontal axis) in separation (top) and position angle (bottom). Asterisks mark the orbits of grades 1, 2, and 3.

tion to the separations  $\rho_{\text{meas}}/\rho_{\text{eph}} = 1.013 \pm 0.018$ . The median values of these calibration parameters are  $4.0^\circ$  and  $1.015$ , respectively. Thus, we revise the pixel scale from the nominal  $15 \text{ mas}$  to  $14.8 \pm 0.2 \text{ mas}$ . The measured positions in Table 2 include these corrections and must be directly comparable with the ephemeris positions. Such a comparison is presented in Fig. 5 for our 10 “calibrators”. The errors in Table 2 *do not include calibration uncertainties* and characterize only internal measurement errors. The calibration errors would otherwise dominate in most cases. If the motion of some pairs is determined with a better accuracy in the future, the data presented here can be corrected accordingly.

Measurement of magnitude differences by speckle interferometry has always been very tricky because the terms  $A$  and  $B$  in the power spectrum

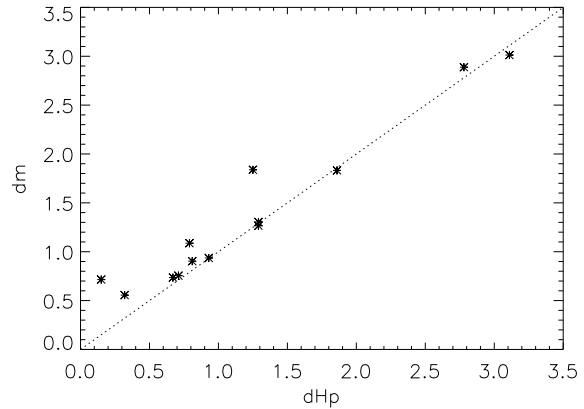


Fig. 6.— Comparison of the magnitude differences  $\Delta H_p$  measured by HIPPARCOS with our results.

(eq. 2) are affected by various biases. Nevertheless, a CCD detector like Luca has a linear response and holds promise of reliable differential photometry. Horch et al. (2004) studied the accuracy of relative speckle photometry with CCD and demonstrated that random errors can be as low as  $0.13^m$ . The  $\Delta m$  of wide pairs is systematically over-estimated because of the anisoplanatism. Perhaps the most reliable differential photometry is provided by HIPPARCOS (ESA 1997), listed as  $\Delta H_p$  in the last column of Table 2. Direct comparison with our results shows overall consistency and some deviant points. (Fig. 6). Some disparity is expected because the passbands are not the same (especially for some early-type components with strong  $H\alpha$  line). Large deviations are commented below.

## 5. Discussion of individual systems

Comments on some binaries are listed below. For stars without comments, the following orbits were used: 01084-5515 – Ling (2004); 01361-2954 – Cvetkovic & Novakovic (2006); 01376-0924 – Tokovinin (1993); 02396-1152 and 04142-4608 – Söderhjelm (1999); 03184-2231 and 05190-2159 – Seymour et al. (2002); 03339-3105 – Heintz (1996).

**00352-0336 = 13 Cet** has a good-quality orbit by Mason & Hartkopf (2005). The pair was caught near the periastron, on a previously unobserved part of its orbit, but still follows the ephemeris. The primary is a 2.1-day spectroscopic

binary (SB).

**00373-2446** shows larger-than-expected deviation in  $\theta$  from the grade 1 combined visual-spectroscopic orbit by Pourbaix (2000).

**02038-0021 = 61 Cet** is a single-lined SB with period 2066 days resolved here for the first time. Griffin (1995) estimated the spectral types of Aa and Ab as G8III and F0V and suggested this object as a likely candidate for resolution. Previous attempt by Sowell et al. (2001) to resolve this composite-spectrum system on a smaller telescope gave negative result. Pourbaix & Boffin (2003) could not derive astrometric orbit by re-processing the HIPPARCOS data. As the separation is close to the diffraction limit, the  $\Delta m$  correlates with  $\rho$  and our estimates of both parameters can be uncertain. There is a physical tertiary component at  $42''.7$ .

**02128-0224 = 66 Cet** is yet another SB in a triple system resolved here for the first time. The F8V components of this 95-day double-lined system (Duquennoy & Mayor 1991) are nearly identical (twins), suggesting  $\Delta m \sim 0$ . We repeated the processing with forced  $\Delta m = 0$  and found very similar results, ( $20.6 \pm 1.1 \text{mas}$ ,  $115.6^\circ \pm 2.7^\circ$ ). The separation is formally below the diffraction limit of SOAR. A physical tertiary is located at  $16''.6$ .

**02225-2349 =  $\kappa$  For** is a bright star with invisible component. Gontcharov & Kiyaveva (2002) proposed an astrometric orbit with a period 26.5 yr and semi-major axis  $\alpha = 0''.26 \pm 0''.01$ . They estimate that the true axis  $a$  might be  $0''.54$  or  $0''.85$ . The smallest of those is used here for calculating the ephemeris. Our measurement is broadly compatible with this orbit. Niedever et al. (2002) monitored precise radial velocity of this star in search for planets and found a linear drift of  $-1.7 \text{m s}^{-1} \text{day}^{-1}$ , confirming the long-period binary nature independently. To our knowledge, the astrometric companion is resolved here for the first time. The component is securely detected in all data cubes (Fig. 3) and its position matches the ephemeris of Gontcharov & Kiyaveva if the semi-major axis is  $a = 0''.68$ . A large ratio between the astrometric and true semi-major axes  $\gamma = \alpha/a = 0.38$  indicates that the secondary companion B is massive,  $q = M_B/M_A = \gamma/(1 - \gamma) = 0.90$ .

There is some uncertainty about the distance to the system. The HIPPARCOS parallax  $\pi_{\text{HIP}} = 45.6 \pm 0.8 \text{mas}$  seems to be reliable, but leads to the total system mass of  $4.8 M_\odot$  if  $a = 0''.68$  is adopted. The primary should then be slightly evolved,  $1.5^m$  above the Main Sequence. However, HIPPARCOS data reduction could be affected by the motion in astrometric orbit, so true parallax could be larger and the mass sum smaller. If we adopt the primary mass  $1.2 M_\odot$ , as appropriate for the spectral type G2V, the total system mass would be  $2.3 M_\odot$  and corresponds to the dynamical parallax  $\pi_{\text{dyn}} = 58 \text{mas}$ . With this parallax, the luminosity of the primary matches its Main Sequence spectral type. The secondary component could be either a massive white dwarf or a close pair of M-type dwarfs. Further study of this interesting system is needed.

**02460-0457** shows a large discrepancy in the separation with respect to the preliminary (grade 5) orbit by Olevic (2002) (see the most deviant point in Fig. 5). Other recent speckle measurements show the same trend. An astrometric subsystem with 36 yr period proposed by Dommanget (1972) was not resolved, while the quality of our fits  $\chi^2/\nu \sim 1$  indicates that the binary-star model is sufficient. The position of the astrometric subsystem predicted for the moment of our observation is ( $0''.044, 21.0^\circ$ ).

**03003-1118** shows a large discrepancy with the orbit by Baize (1988), calling for its revision. This  $V = 9.26^m$  star is still well above our sensitivity limit.

**03184-2231** demonstrates a good agreement with the orbit of Seymour et al. (2002). The discrepancy in  $\Delta m$  with HIPPARCOS is likely caused by the  $\text{H}\alpha$  emission of the B9 primary.

**03244-1539** is unresolved, in contradiction with the old orbit by Muller (1955). Hartkopf et al. (2001) note that “There are many negative observations. Needs speckle.”

**03339-5234 = HIP 19248** was resolved with AO in 2004 (Tokovinin et al. 2006), but unresolved here. Apparently, in the visible  $\Delta m$  is too large.

**03544-4022** is a close visual binary with a likely short period of  $\sim 25$  yr but no orbit yet and only few speckle measurements. The spectrum is composite, K0III+A3V. It is not established if the

distant visual companion at  $23''2$  is physically related.

**04395-4507** does not match well its orbit by Söderhjelm (1999). We measure a larger  $\Delta m$  compared to HIPPARCOS, possibly because the noise bias was not completely removed in this  $V = 8.92^m$  object.

**04515-3454** is found much closer than predicted by Heintz (1993).

**05045-3542** =  $\gamma^2$  **Cae** was observed as a reference star but was seen to be a binary. We found later that the companion has already been resolved by HIPPARCOS at ( $0''890, 183.0^\circ$ ), so the true position angle is likely  $191.9^\circ$ . Horch et al. (2001) measured the magnitude difference with speckle method at small telescopes:  $\Delta V = 2.74$ ,  $\Delta R = 2.94$ .

**05239-0052** = **A 847BC** belongs to the quadruple system ADS 3991 where the visual primary component A, at  $2''7$  from BC, is a 22.6-day SB (Tokovinin 1997). The 48-yr orbit of BC by Hartkopf (2000) does not match well our observation. Hartkopf notes that an alternative solution with 24.7-yr period is possible.

**05245-0224** = **McA 18Aa** is a visual-spectroscopic sub-system with orbital period 9.44 yr in a multiple star  $\eta$  Ori. The primary is a 8-day SB. Our measurement matches well the orbit by Olevic & Jovanovic (1998). Schöller et al. (1998) measured the magnitude difference  $\Delta R = 1.41$ , in excellent agreement with our estimate  $\Delta m = 1.48$ . We also note the fainter component B at  $1''7$  in our images.

**05319-7620** =  $\gamma$  **Men** is unresolved despite the separation predicted by the astrometric orbit (Goldin & Makarov 2006), presumably due to the large  $\Delta m$ .

**05532-6150**: our measurement and recent speckle data do not match the orbit by Heintz (1993).

**06003-3102** is the quadruple nearby star Gliese 225.2 (Tokovinin et al. 2005). The new measurement of AB confirms its recently revised orbit. We also observed the sub-system CE and found a marginal signal at the expected companion separation. The CE ephemeris is calculated from the astrometric orbit by assuming a semi-major axis  $0''6$ . Obviously, the mismatch in  $\theta$  between the ephemeris and the observation is very

large, but, on the other hand, the astrometric orbit is still very preliminary, while the companion was found in 2004.861 at a similar position angle, ( $0''514, 145.16^\circ$ ). If the companion is an artefact, we do not find similar artefacts in the reference stars or in the unresolved source of comparable brightness HIP 19248. Tokovinin et al. (2005) note anomalously “blue”  $J - K$  color of the component E, its magnitude difference with C in  $J$  and  $K_s$  bands being the same,  $2.65^m$ . We measure  $\Delta m = 3.9$  at 657 nm, so the E component is redder than C in the visible.

**22266-1645** = **53 Aqr** has a strong weight in the calibration of these data, despite poor quality of its orbit (Hale 1994). We also note a large discrepancy in  $\Delta m$  with HIPPARCOS, although all our measurements are internally consistent. A relatively large separation of this pair leads to the reduced speckle correlation due to anisoplanatism, see Horch et al. (2004). Indeed, on the averaged image the components are partially resolved and their nearly equal intensity is obvious.

## 6. Conclusions

Our first test run of HRCam has unexpectedly produced some interesting results. We resolved three systems for the first time. For a number of other binaries, we find significant discrepancies with their orbits. We tried to observe bright southern stars with known orbits and immediately realized the scarcity of such objects compared to their northern counterparts. Southern binaries remain largely neglected, and a speckle program on 4-m telescope can significantly improve the situation.

The limiting magnitude of the HRCam was not explored during this run. It is clear that we can go fainter by increasing spectral bandwidth or exposure time and by accumulating longer. However, we resolved a couple of binaries with  $V = 9^m$  easily. Thus, we can expect that stars down to  $V = 12^m$  can be observed with HRCam, as with other speckle systems. Even fainter stars will become accessible in the future with partial AO correction provided by SAM.

We thank the SOAR telescope team for the possibility of testing HRCam on technical night and for their help in installing the instrument. The

telescope was operated by S. Pizarro and D. Maturana. This research has made use of the CDS and SIMBAD services and of the Washington Double Star Catalog maintained at the U.S. Naval Observatory.

## REFERENCES

- Altarac, S., Berlioz-Arthaud, P., Thiébaud, E., Foy, R., Balega, Y.Y., Dainty, J.C., & Fuenzalida, J.J. 2001, MNRAS, 322, 141
- Baize, P. 1988, A&AS 74, 507
- Cecil, G., & Rashkeev, D. 2007, AJ, 134, 1468
- Cvetkovic, Z., & Novakovic, B. 2006, Serbian Astron. J., 173, 73,
- Dainty, J.C., & Greenaway, A.H. 1979, J. Opt. Soc. Am., 69, 786
- Dommanget, J. 1972, Bull. R. Astron. Obs. Belgium, 8, 63-66
- Duquenooy, A., & Mayor, M. 1991, A&A, 248, 485
- ESA 1997, European Space Agency, SP-1200
- Goldin, A., & Makarov, V.V. 2006, ApJS, 166, 341
- Gontcharov, G.A., & Kiyaveva, O.V. 2002, AstL, 28, 261
- Griffin, R.F. 1995, Obs., 115, 84
- Hale, A. 1994, AJ, 107, 306
- Hartkopf, W.I. 2000, IAU Comm. 26. Inf. Circ. 141
- Hartkopf, W.I., Mason, B.D., & Worley, C.E. 2001, AJ, 122, 3472  
<http://www.ad.usno.navy.mil/wds/orb6/orb6.html>
- Heintz, W.D. 1993, A&AS, 98, 209
- Heintz, W.D. 1996, AJ, 111, 412
- Horch, E.P., Ninkov, Z., & Slawson, R.W. 1997, AJ, 114, 2117
- Horch, E., Ninkov, Z., & Franz, O.G. 2001, AJ, 121, 1583
- Horch, E.P., Meyer, R.D., van Altena, W.F. 2004, AJ, 127, 1727
- Ling, J.F. 2004, AJ, 153, 545
- Muller, P. 1955, J. Obs., 38, 17
- Mason, B.D., Wycoff, G.L., Hartkopf, W.I., Douglas, G.G., & Worley, C.E. 2001, AJ, 122, 3466  
<http://ad.usno.navy.mil/wds/>
- Mason, B.D. & Hartkopf, W.I. 2005, IAU Comm. 26. Inf. Circ. 156
- Nieverder, D.L., Marcy, G.W., Butler, R.P., Fisher, D.A., & Vogt, S.S. 2002, ApJS, 141, 503
- Olevic, D., & Jovanovic, P. 1998, IAU Comm. 26. Inf. Circ. 136
- Olevic, D. 2002, IAU Comm. 26. Inf. Circ. 148
- Pourbaix, D. 2000, A&AS, 145, 215
- Pourbaix, D., & Boffin, H.M.J. 2003, A&A, 398, 1163
- Press, W.H., Teukolsky, S.A., Vetterling, W.T., & Flannery, B.P. 1992, Numerical Recipes in C (2nd ed; Cambridge: Cambridge Univ. Press)
- Schöller, M., Balega, I.I., Balega, Y.Y., Hofmann, K.-H., Reinheimer, T., & Weigelt, G. 1998, AstL, 24, 283
- Seymour, D.L., Mason, B.D., Hartkopf, W.I., & Wycoff, G.L. 2002, AJ, 123, 1023
- Söderhjelm, S. 1999, A&A, 341, 121
- Sowell, J.R., Bord, D.J., Hart, D.L., & Beletic, J.W. 2001, AJ, 122, 1981
- Tokovinin, A.A. 1993, SvAL, 19, 73
- Tokovinin, A. 1997, A&AS, 121, 71
- Tokovinin, A., Thomas, S., Gregory, B., van der Bliik, N., Schurter, P., Cantarutti, R., & Mondaca, E. 2004, in: Advancements in adaptive optics, eds. Bonaccini Calia, D., Ellerbroek, B.E., Ragazzoni, R., Proc. SPIE, 2004, 5490, 870
- Tokovinin, A.A., Kiyaveva, O., Sterzik, M., Orlov, V., Rubinov, A., & Zhuchkov, R. 2005, A&A, 441, 695
- Tokovinin, A., Thomas, S., Sterzik, M., & Udry, S. 2006, A&A, 450, 681

---

This 2-column preprint was prepared with the AAS L<sup>A</sup>T<sub>E</sub>X

